INTERNATIONAL JOURNAL FOR NUMERICAL METHODS IN FLUIDS
Int. J. Numer. Meth. Fluids 2001; **37**: 399–418 (DOI: 10.1002/fld.181)

A Lagrangian boundary element approach to transient three-dimensional free surface flow in thin cavities

Jie Zhang and Roger E. Khayat*,[1]

Department of Mechanical and Materials Engineering, University of Western Ontario, London, Ontario, Canada

SUMMARY

The lubrication theory is extended for transient free-surface flow of a viscous fluid inside a three-dimensional thin cavity. The problem is closely related to the filling stage during the injection molding process. The pressure, which in this case is governed by the Laplace's equation, is determined using the boundary element method. A fully Lagrangian approach is implemented for the tracking of the evolving free surface. The domain of computation is the projection of the physical domain onto the (x, y) plane. This approach is valid for simple and complex cavities as illustrated for the cases of a flat plate and a curved plate. It is found that the flow behavior is strongly influenced by the shape of the initial fluid domain, the shape of the cavity, and inlet flow pressure. Copyright © 2001 John Wiley & Sons, Ltd.

KEY WORDS: boundary element; free-surface; injection molding; thin cavity flow

1. INTRODUCTION

This study examines the numerical solution for a viscous incompressible fluid flowing inside a three-dimensional thin cavity, with special emphasis on the filling stage of the injection molding process. A wide range of flow problems in polymer processing involve the presence of a free surface. In some processes such as blow molding, thermoforming and conventional injection molding, the flow is strictly unsteady. In other processes, such as film blowing, wire coating and extrusion, most of the interest lies in the long-term behavior, after transients have died out. The flow may then be studied in the steady state regime.

The numerical simulation of free surface flow problems remains challenging despite the advent of powerful techniques. Typically, a flow problem of the moving type, which involves geometrical non-linearities, must be addressed. In contrast to conventional problems in fluid dynamics, the domain of computation, which is bounded in part by the free surface, is not known *a priori* since the shape of the free surface itself must be determined as part of the

* Correspondence to: Department of Mechanical and Materials Engineering, University of Western Ontario, London, Ontario N6A 5B9, Canada.
[1] E-mail: rkhayat@eng.uwo.ca

Received February 2000
Accepted September 2000

solution. In steady state problems, a number of iterations are usually needed in order to reach the precise form of the free surface. The problem becomes even more challenging when in addition the shape of the free surface evolves with time, generating large distortions in the discretized domain of the fluid. While large distortions have been reasonably well handled for two-dimensional free surface flows, major issues remain open regarding complex three-dimensional problems.

Several numerical techniques have been developed for the solution of moving boundary/initial value problems. These techniques may be classified as Eulerian, Lagrangian, and mixed Eulerian–Lagrangian [1]. In the Eulerian description of the flow, the grid points remain stationary or move in a predetermined manner [2–5]. Typically, the fluid moves in and out of the computational cells. The method can handle arbitrarily large free surface deformations without loss of accuracy. Its main disadvantage, however, is the lack of sharp definition of the free surface, and the consequent difficulty to impose the kinematic and dynamic boundary conditions on the free surface. In the Lagrangian approach, the grid points move with local fluid particle [6,7]. The free surface is sharply defined and it is easy to impose the necessary boundary conditions. However, Lagrangian methods require mesh refinement or remeshing for large deformations of the free surface. Hybrid methods have also been developed that combine the advantages of the Eulerian and Lagrangian methods [8].

More recently, some of the basic techniques have been improved. Peterson *et al.* [9] proposed an iterative automatic mesh generation for a free-surface flow in an initially arbitrary domain. A second-order model based on the volume-of-fluid method was proposed by Kim and No [10] for free surface convection and interface reconstruction. The methodology defines the second-order linear curve having both face slopes as near horizontal as possible while satisfying the cell's defined volume fraction [10]. In free surface flow, the determination of the normal vector and its gradient is crucial for front advanced and the inclusion of surface-tension effect. In this regard, Engelman and Sani [11] introduced the notion of mass-consistent normal free-surface flow. Other techniques have also been developed in relation to drop deformation and interfacial phenomena. Mashayek and Asgriz [12] proposed a spine-flux method, which is based on discretizing the liquid surface by a spine function, and spine subdivision of the liquid zone into conical sub-volumes. The problems of drop oscillation and drop collision were examined. The analysis of capillary-driven flow during sintering was carried out by Martinez-Herrera and Derby [13] using a front-tracking method coupled with algebraic mesh generation. The formation of a drop of liquid from a capillary tube into an ambient gas phase was studied by Wilkes *et al.* [14]. A finite element algorithm was implemented, which incorporates a multiregion mesh that conforms to and evolves with the changing shape of the drop. Finally, Levesque and Li [15] presented a second-order accurate interface tracking method for the solution of Stokes flow with elastic boundaries or surface tension. The interface is represented by a cubic spline along which the singularity supported elastic or surface tension force could be computed.

Generally, an adaptive Lagrangian approach becomes difficult to implement when a volume method such as the finite element method (FEM) is used. On the other hand, the boundary element method (BEM) is much easier to use along with adaptive remeshing as the dimension of the problem is reduced by one. The BEM relates velocities at points within the fluid to the velocity and stress on the bounding surfaces. It is thus an ideal method for studying

moving-boundary problems where the velocity on the moving boundary is the quantity of prime interest. The advantages of the BEM include: reduction of problem dimensionality, direct calculation of the velocity at the moving boundary, the ability to track large surface deformations, and the potential for easy incorporation of interfacial tension as well as other surface effects. Recent studies by Khayat and co-workers on the applicability of the BEM to problems of the moving-boundary type include the deformation of a drop in a confined medium of Newtonian and non-Newtonian systems [16–21], conventional and gas-assisted injection molding [22,23], air venting during blow molding and thermoforming [24], and the transient mixing of Newtonian and viscoelastic fluids [25,26]. Khayat and Marek [27] developed an adaptive three-dimensional BEM for the transient free surface in a confined medium. The formulation and numerical implementation are illustrated for a flow advancing inside and exiting a confining cavity, typically as the flow is encountered in extrusion. The method was also used to examine the three-dimensional deformation of a drop in viscoelastic systems [20].

The present study focuses on the flow inside a three-dimensional thin cavity, typically as this flow is encountered during the filling stage in injection molding or through the die at the exit of an extruder. However, shear-thinning and viscoelastic effects are not accounted for in this study. While the BEM has obvious advantages over conventional domain methods for the treatment of moving domain flows, it suffers from severe drawbacks. A number of simplifying assumptions must be adopted for the BEM to become applicable. Despite the advent of recent non-linear BEM techniques [28–31], the method remains seriously challenged by conventional approaches in its capability to handle transient and non-linear problems. The inherent transient nature of the flow process and the presence of a moving free surface make the simulation of the problem challenging because of the geometrical non-linearities involved [1]. The challenge becomes even greater if inertia or non-Newtonian effects are included. Such non-linear phenomena have been addressed in moving-boundary problems with relevance to polymer processing [32–35]. However, these problems were limited to simple flow configurations, and definitely to two-dimensional or axisymmetric flows. Viscoelastic effects were examined, for instance, on the growth of spherical and cylindrical shells of a fluid obeying a highly non-linear viscoelastic constitutive model [34]. The deformation of a viscoelastic column was also examined [35].

2. PROBLEM FORMULATION

In this section, the basic assumptions for the lubrication equations are first briefly reviewed for viscous fluids. The theory is then extended to include the transient free surface flow inside thin three-dimensional cavities.

2.1. General equations, initial and boundary conditions

Consider an incompressible Newtonian fluid of density ρ, viscosity μ, and surface tension coefficient γ. Gravity effect is assumed to be negligible. If (x_1, x_2, x_3) denotes the three-dimensional system of Cartesian co-ordinates, with $\mathbf{x}$ being the position vector, then the conservation equations for an incompressible fluid can be concisely written as:

$$\nabla\cdot\mathbf{u} = 0, \qquad \rho(\mathbf{u}_{,T} + \mathbf{u}\cdot\nabla\mathbf{u}) = -\nabla P + \mu\nabla^2\mathbf{u} \tag{1}$$

where a subscript after a comma denotes partial differentiation, $\mathbf{u}(u_1, u_2, u_3)$ is the velocity vector, P is the pressure, T is the time, and ∇ is the gradient operator.

The lubrication assumption is the hydrodynamic analog of shell theory for solids. In most lubrication films the thickness of the film is small compared with its lateral dimensions. Properly handled, this observation can be used to eliminate from the hydrodynamic equations and boundary conditions the dependence upon one of the three spatial variables. The continuity equation is integrated across the film and the Navier–Stokes equation is used to evaluate the quantities appearing as integrands. Consider the flow of a thin continuous film of incompressible fluid between two rigid surfaces $x_3 = F_1(x_1, x_2)$ and $x_3 = F_2(x_1, x_2)$. Then the film thickness is defined by

$$H(x_1, x_2) = F_2(x_1, x_2) - F_1(x_1, x_2) \tag{2}$$

The conservation Equations (1) are now formulated in the narrow-gap limit. It is convenient to cast these equations in terms of dimensionless variables. Typically, in thin-cavity flow, there are three characteristic lengths, L_1 and L_2 along the lateral directions x_1 and x_2, and H_0, which represents the thickness of the cavity in the x_3-direction. Figure 1 illustrates schematically the general flow and notations used. The figure shows a step of the filling stage of a thin cavity of general shape. The fluid is assumed to occupy a simply-connected region, $\Omega(t)$, which is bounded by $\Gamma(t)$. The boundary consists of the moving free surface or front, $\Gamma_f(t)$, the wetted part of the cavity, $\Gamma_w(t)$, and a source region, Γ_s, at the entrance to the cavity.

The fluid is assumed to be initially at rest, so that

$$\mathbf{u}(\mathbf{x}, t = 0) = 0, \quad \mathbf{x}\in\Omega(t = 0) \tag{3}$$

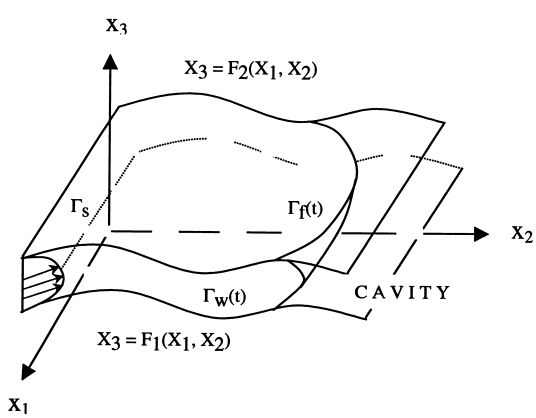

Figure 1. Schematic illustrating the transient free-surface flow inside a cavity induced by the imposed flow at the source boundary, Γ_s.

The boundary conditions are prescribed as follows. The fluid is assumed to adhere to the top and bottom cavity surfaces

$$\mathbf{u}(\mathbf{x}, t) = 0, \qquad x_3 = F_1(x_1, x_2) \text{ or } F_2(x_1, x_2) \tag{4}$$

On the lateral sides of the cavity, the lubrication assumption can only accommodate the no-penetration condition, but the fluid is forced to slip. The free surface is given by $x_1 = F(x_1, x_2, t)$, so that the evolution of the front is dictated by the kinematic condition

$$u_1(x_1 = F, x_2, x_3, t) = \frac{\mathrm{d}F}{\mathrm{d}t}(x_2, x_3, t) \tag{5}$$

and the dynamic condition expresses the traction in terms of surface-tension effects, reading

$$-p\mathbf{n} + \mu[\nabla\mathbf{u} + (\nabla\mathbf{u})^t]\cdot\mathbf{n} = -\gamma(\nabla\cdot\mathbf{n})\mathbf{n}, \quad \mathbf{x}\in\Gamma_f(t) \tag{6}$$

where $\mathbf{n}(x, t)$ is the normal vector to the free surface, and the superscript t denotes matrix transposition. Finally, it is noted that the flow is induced by an applied flow rate at the boundary source, Γ_s.

2.2. Lubrication equations and boundary conditions

The problem above is now formulated in the narrow-gap limit. In this study, L_1 and L_2 will be taken to be of the same order, L, so that the dimensionless variables may be introduced as follows

$$\begin{aligned} &(x, y) = \frac{1}{L}(x_1, x_2), \qquad z = \frac{x_3}{H_0}, \qquad t = \frac{V}{L}T, \\ &(u_x, u_y) = \frac{1}{V}(u_1, u_2), \quad u_z = \frac{L}{VH_0}u_3, \quad p = \left(\frac{H_0}{L}\right)^2 \frac{L}{\mu V}P, \end{aligned} \tag{7}$$

where V is a typical (reference) velocity. Three important dimensionless groups emerge in the problem, namely, the aspect ratio, ε, the Reynolds number, Re, and the capillary number, Ca:

$$Re = \frac{\rho VL}{\mu}, \qquad \varepsilon = \frac{H_0}{L}, \qquad Ca = \frac{\mu V}{\gamma} \tag{8}$$

In dimensionless form, and if terms of $O(\varepsilon^2)$ and higher are excluded, then the conservation equations in (1) reduce to

$$u_{\alpha,\alpha} + u_{z,z} = 0 \tag{9}$$

$$\varepsilon^2 Re(u_{\alpha,t} + u_j u_{\alpha,j}) = -p_{,\alpha} + u_{\alpha,zz}, \qquad p_{,z} = 0 \tag{10}$$

where a Greek index corresponds to x and y, and a Latin index corresponds to x, y and z. Note that the term $\varepsilon^2 Re$ is not necessarily negligible since Re may be large enough for this term to be of order one. However, for most polymeric flows, the Reynolds number is small enough for inertia effects to be negligible. This is more so for the flow in a thin cavity since $\varepsilon \ll 1$. In this case, the momentum equation is integrated along z to give:

$$u_\alpha = \frac{p_{,\alpha}}{2}(z - h_2)(z - h_1) \tag{11}$$

where $h_1 = F_1/H_0$ and $h_2 = F_2/H_0$ are the dimensionless heights of the lower and upper rigid surfaces respectively. If the continuity equation is integrated between $z = h_1$ and $z = h_2$, and expression (11) is used, then the following equation for the pressure is obtained

$$(h^3 p_{,x})_{,x} + (h^3 p_{,y})_{,y} = 0 \tag{12}$$

where $h = H/H_0$ is the dimensionless thickness of the cavity. If the thickness is constant, then the pressure is dictated by the Laplace's equation

$$p_{,xx} + p_{,yy} = 0 \tag{13}$$

Most cavities of practical interest have a constant thickness, particularly in relation to injection molding. For simplicity, in this work, h will then be assumed to be constant. The problem thus reduces to solving the Laplace's equation (13) in the (x, y) plane.

Regarding the boundary conditions, the lubrication formulation does not accommodate adherence conditions at the lateral walls, at $x_2 = 0$ and $x_2 = L_2$ (for straight lateral walls). Stick boundary conditions can only be applied at the bottom and upper surfaces, $x_3 = F_1$ and $x_3 = F_2$ respectively. In this case, only the no-penetration condition applies along the lateral walls. The flow is assumed to be driven by an imposed (dimensionless) pressure gradient, $q_0(y, z, t)$, at $x = 0$, so that the general boundary condition at the entrance to the cavity is given by

$$q(x = 0, y, z, t) = q_0(y, z, t) \tag{14}$$

where $q = \mathbf{n} \cdot \nabla p$ is the normal derivative of the pressure. The pressure gradient may be either maintained fixed at all time, or adjusted according to the flow conditions inside the cavity (mold). A time-dependent pressure gradient corresponds typically to the inlet condition in injection molding where the pressure rather than the flow rate is varied with time at the source of fluid. Although a variable pressure gradient can be easily accommodated by the present formulation, q_0 will be assumed to depend only on y. Since the lubrication assumption can only accommodate the no-penetration conditions at the lateral walls, then

$$\mathbf{n}(\mathbf{x}, t) \cdot \nabla p(\mathbf{x}, t) = 0, \quad \mathbf{x} \in \Gamma_w(t) \tag{15}$$

where $\mathbf{n}$ is the unit normal to $\Gamma_w(t)$.

At the front (free surface) the imposition of a suitable dynamic condition is not obvious for thin-cavity flow. It is clear from condition (6) that for the general three-dimensional flow, and in the absence of surface tension effect, a zero-traction condition must apply at the front. Consider now the dynamic condition at the front, which, in dimensionless form, is represented by $x = X(y, z, t)$ for $z \in [h_1, h_2]$, and $t > 0$. Let $\mathbf{n}(y, z, t)$ be the unit normal vector to the front. The dynamic condition (6) at $x = X(y, z, t)$ becomes, upon projection in the lateral directions

$$pn_\alpha - \varepsilon^2(u_{\alpha,\beta} + u_{\beta,\alpha})n_\beta - \varepsilon u_{\alpha,z}n_z = \frac{\varepsilon}{Ca}(\varepsilon n_{\beta,\beta} + n_{z,z})n_\alpha \tag{16}$$

and in the transverse direction

$$pn_z - \varepsilon u_{\beta,z} - 2\varepsilon^2 u_{z,z} = \frac{\varepsilon}{Ca}(\varepsilon n_{\beta,\beta} + n_{z,z})n_z \tag{17}$$

Higher-order terms in Equations (16) and (17) can only be identified once the expressions for the normal vector components and their derivatives are given explicitly. For a point (x, y, z) that belongs to the free surface, the components of the normal vector must satisfy

$$n_x\,\mathrm{d}x + n_y\,\mathrm{d}y + \varepsilon n_z\,\mathrm{d}z = 0 \tag{18}$$

The kinematic condition at the front

$$\frac{\mathrm{d}x}{\mathrm{d}t} = \frac{\mathrm{d}X}{\mathrm{d}t}$$

also gives

$$\mathrm{d}x - X_{,y}\mathrm{d}y - X_{,z}\mathrm{d}z - X_{,t}\mathrm{d}t = 0 \tag{19}$$

The differential $\mathrm{d}t$ can be expressed in terms of $\mathrm{d}x$ and $\mathrm{d}y$ by noting that, at the free surface

$$u = \frac{\mathrm{d}X(y, z, t)}{\mathrm{d}t} \tag{20}$$

which leads to

$$\mathrm{d}t = \left(\frac{X_{,y}}{u - X_{,t}}\right)\mathrm{d}y + \left(\frac{X_{,z}}{u - X_{,t}}\right)\mathrm{d}z \tag{21}$$

Substituting for $\mathrm{d}t$ from Equation (21) into Equation (19), and comparing the resulting equation with Equation (18) give the (normalized) components of the unit normal vector to leading order in ε

$$n_x \approx \varepsilon\left(\frac{u - X_{,t}}{X_{,z}}\right), \qquad n_y \approx -\varepsilon\frac{uX_{,y}}{X_{,z}}, \qquad n_z \approx -u \tag{22}$$

It is not difficult to conclude that, to leading order in ε, and upon substituting expressions (22) into Equations (16) and (17), Equation (16) is readily satisfied, and Equation (17) leads to the vanishing of the pressure at the free surface

$$p(x = X, y, z, t) = 0 \tag{23}$$

In reaching condition (23), it is assumed that $Ca \sim O(1)$. In fact, for polymeric fluids, Ca is large enough for surface-tension effects to be negligible. Finally, the remaining boundary condition is the kinematic condition at the free surface, which is the least obvious among the boundary conditions to implement. The kinematic condition relates the evolution of the free surface to the local velocity field. The free surface deforms in accord with the instantaneous and local velocity field, thus determining new free surface positions with time. In a Lagrangian representation, such as the present formulation, the moving boundary may be assumed to deform with the fluid velocity, such that the evolution of $\Gamma_f(t)$ is governed by the equation

$$\frac{d\mathbf{x}}{dt} = \mathbf{u}(\mathbf{x}, t), \quad \mathbf{x} \in \Gamma_f(t) \tag{24}$$

Although easy to implement, the resulting scheme based on Equation (24) tends to sweep points on the moving boundary along the tangent to the moving boundary, even if only small shape changes take place. Consequently, frequent redistribution of the moving boundary points or remeshing would be necessary to implement.

Alternatively, and in this paper, the free surface is assumed to deform pointwise along the normal with the normal projection of the fluid velocity at the free surface [1]. This method keeps the points evenly distributed on the free surface. Thus, the following kinematic boundary condition is assumed to hold on $\Gamma_f(t)$

$$\frac{d\mathbf{x}}{dt} = \mathbf{n}(\mathbf{x}, t)[\mathbf{n}(\mathbf{x}, t) \cdot \mathbf{u}(\mathbf{x}, t)], \quad \mathbf{x} \in \Gamma_f(t) \tag{25}$$

The form (25) is particularly suited when a boundary element approach is used as will be observed next.

3. SOLUTION PROCEDURE

In this section, the boundary integral equation is briefly reviewed in the context of free-surface flow. The front-tracking scheme is discussed in some detail. The domain of computation will be the projection, $\Omega_{xy}(t)$, in the (x, y) plane, of $\Omega(t)$ occupied by the fluid at time t. For convenience, the subscript xy will be dropped.

3.1. Boundary integral equation

The general boundary integral equation for a point $\mathbf{x}(x, y) \in \Omega(t) \cup \Gamma(t)$ is simply stated [36]

$$c(\mathbf{x}, t)p(\mathbf{x}, t) + \int_{\Gamma(t)} p(\mathbf{y}, t)q^*(\mathbf{x}|\mathbf{y})\, d\Gamma_{\mathbf{y}} - \int_{\Gamma(t)} q(\mathbf{y}, t)p^*(\mathbf{x}|\mathbf{y})\, d\Gamma_{\mathbf{y}} = 0 \tag{26}$$

where $q(\mathbf{x}, t) = \mathbf{n}(\mathbf{x}, t)\cdot\nabla p(\mathbf{x}, t)$ is the normal derivative of the pressure, $\Gamma(t)$ is the boundary surrounding the domain $\Omega(t)$, and $c(\mathbf{x}, t) = 1$ for $\mathbf{x} \in \Omega(t)$ and $c(\mathbf{x}, t) = 1/2$ for $\mathbf{x} \in \Gamma(t)$ if the boundary is (Lyapunov) smooth. The fundamental pressure and normal derivative solutions to the problem are given by

$$p^*(\mathbf{x}|\mathbf{y}) = \frac{1}{4\pi|\mathbf{x} - \mathbf{y}|}, \qquad q^*(\mathbf{x}|\mathbf{y}) = \mathbf{n}(\mathbf{y}, t)\cdot\nabla p^*(\mathbf{x}|\mathbf{y}) \tag{27}$$

Note that $\mathbf{n}(\mathbf{x}, t)$ is the outward unit normal vector to the boundary. Equation (26) is rewritten more explicitly once the boundary conditions on $\Gamma(t) = \Gamma_s \cup \Gamma_w(t) \cup \Gamma_f(t)$, are applied. It is recalled that Γ_s is the source part of the boundary, where $q = q_s(\mathbf{x})$, $\Gamma_w(t)$ is the wetted wall where $q = 0$, and $\Gamma_f(t)$ is the front where $p = 0$. Thus, at the wall, for $\mathbf{x} \in \Gamma_s \cup \Gamma_w(t)$, Equation (26) reduces to

$$c(\mathbf{x}, t)p(\mathbf{x}, t) + \int_{\Gamma_w(t) \cup \Gamma_s} p(\mathbf{y}, t)q^*(\mathbf{x}|\mathbf{y})\, d\Gamma_{\mathbf{y}} - \int_{\Gamma_f(t)} q(\mathbf{y}, t)p^*(\mathbf{x}|\mathbf{y})\, d\Gamma_{\mathbf{y}} = \int_{\Gamma_s} q_s(\mathbf{y})p^*(\mathbf{x}|\mathbf{y})\, d\Gamma_{\mathbf{y}} \tag{28}$$

and at the front, for $\mathbf{x} \in \Gamma_f(t)$, one has

$$\int_{\Gamma_w(t) \cup \Gamma_s} p(\mathbf{y}, t)q^*(\mathbf{x}|\mathbf{y})\, d\Gamma_{\mathbf{y}} - \int_{\Gamma_f(t)} q(\mathbf{y}, t)p^*(\mathbf{x}|\mathbf{y})\, d\Gamma_{\mathbf{y}} = \int_{\Gamma_s} q_s(\mathbf{y})p^*(\mathbf{x}|\mathbf{y})\, d\Gamma_{\mathbf{y}} \tag{29}$$

It is Equation (29) that is of particular interest since it allows the determination of $q(\mathbf{x} \in \Omega_f, t)$, which, in turn and through (11), yields the value of the velocity at the front. The equation must, however, be solved simultaneously with Equation (28).

When the boundary is Lyapunov smooth, which requires that a local tangent to the free surface exists everywhere, the function $c(\mathbf{x}, t) = 1/2$. This is the case if linear boundary elements are used. Thus, the assumption of boundary smoothness is generally not valid in the vicinity of sharp corners, cusps or edges. In general, since $c(\mathbf{x}, t)$ depends solely on geometry, it may be evaluated assuming that a uniform pressure field such as $p(\mathbf{x}, t) = 1$ is applied over the boundary. Under these conditions, all derivatives (including q) must vanish. Hence, at any time t, Equation (28) reduces to

$$c(\mathbf{x}, t) = -\int_{\Gamma_w(t) \cup \Gamma_s \cup \Gamma_f(t)} q^*(\mathbf{x}|\mathbf{y})\, d\Gamma_{\mathbf{y}} \tag{30}$$

Thus, at any time t, the form of the boundary $\Gamma(t)$ is determined, and the function $c(\mathbf{x}, t)$ is evaluated using the equation above.

3.2. Discretization and front tracking

The solution of Equations (28) and (29) is very similar to that of the integral equation in potential theory. In the present case, however, the domain changes with time. Linear segments are used in the discretization of $\Gamma(t)$ since they can yield an arbitrary degree of accuracy by increasing the number of boundary elements. An Eulerian finite difference scheme is implemented to solve Equation (25) and update the front position once $q(\mathbf{x}\in\Gamma_f, t)$ is determined at a given time step. If the expression (11) for the velocity is applied at the front, and is substituted into Equation (25), one has the following equation

$$\frac{d\mathbf{x}}{dt} = q(\mathbf{x}, t)(z-h_1)(z-h_2)\mathbf{n}(\mathbf{x}, t)/2, \quad \mathbf{x}\in\Gamma_i(t) \tag{31}$$

which governs the evolution of the front at a given height, z. It must understood that $\mathbf{x}$ in Equation (31) is the position vector of a point at the front in the (x, y) plane. Since for linear segments, the BEM yields the values of the velocity and traction at the centroid of the segments, the velocity and normal vectors at the nodes are computed by simply taking the average over the two connecting segments. More accurate evaluation of nodal values are of course possible, by either increasing the order of the boundary elements or using higher-order interpolation. For example, Engelman *et al.* introduced the notion of mass-consistent normals for the same type of problem [10].

4. NUMERICAL ASSESSMENT AND RESULTS

The formulation and numerical solution procedure are now applied to the transient free-surface flow inside thin cavities. Two illustrations are covered: the flow inside a flat cavity, and the flow inside a curved cavity. All results are given in terms of dimensionless quantities. The accuracy and convergence of the method are also assessed.

4.1. Transient flow inside a flat cavity and numerical assessment

Consider the flow inside a flat cavity of constant thickness. The cavity has a length-to-width ratio equal to 4/3. The length and the width are taken to lie along the x- and y-directions respectively, and the fluid flows predominantly in the x-direction, with a strong secondary flow in the y-direction. The projected initial domain occupied by the fluid is given by $x = y(y-2)$ for $y\in[0, 2]$. Figure 2 shows the evolution of the front in the mid-plane ($z = 0.5$) between the two flat plates. The front is shown at equal time intervals of 0.25 units, over a period of 25 time units. The initial domain is included in the figure. Note that the fluid at the points (0, 0) and (0, 2) is assumed to adhere to the $x = 0$ line. In the early stages of flow, the fluid has a relatively strong lateral movement as reflected by the second position of the front, which indicates that the fluid will have contacted the lateral walls in less than 1 time unit. It is

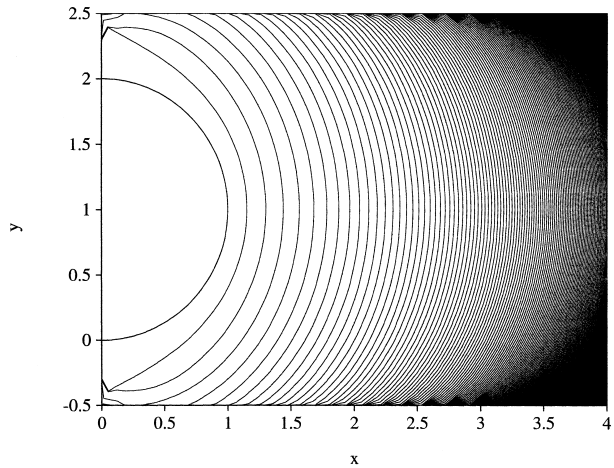

Figure 2. Transient flow inside a flat plate with initial rectangular domain. The fronts are shown at equal time intervals over a period of 25 time units.

interesting to observe from Figure 2 that the first contact between fluid and lateral walls does not occur at $x = 0$, but at roughly $x = 0.25$. The lateral movement continues to expand the fluid until the corners $(0, -0.5)$ and $(0, 2.5)$ are covered, which happens at a time $t < 0.5$. The figure indicates that the spacing between two successive fronts diminishes with time, which means that the fluid becomes harder to drive with time. This is of course expected in this case given the (time) constant flow rate that is imposed at the entrance. In practice, however, such as in injection molding, the pressure gradient is adjusted with time for a desired rate of cavity filling.

A better quantitative assessment is possible by monitoring the time evolution of the front tip position, $X_{\max}(t)$, and the evolution of the contact point, $X_c(t)$. The evolution of the two points is depicted from Figure 3 over 25 time units. The starting point, at $t = 0$, is $X_{\max} = 1$ for the front tip, corresponding to the initial fluid domain shown in the figure. The front evolves initially very fast, as indicated by the relatively large acceleration from the $X_{\max}$ curve, and reaches the opposite cavity wall at $x = 4$ at $t = 10$. There is a significant deceleration before the fluid reaches the opposite wall. The upper constant line in the figure ($X_{\max} = 4$) indicates that the front tip is no longer moving for $t > 10$. The rest of the fluid, however, is still moving for $t > 10$, as indicated by the evolution of the contact point position, X_c, in the figure. The fluid comes in contact with the lateral walls early, at $t = 0.8$. X_c then evolves similarly to but at a slower rate than $X_{\max}$, and reaches the opposite cavity wall at roughly $t = 25$, a time at which the filling is considered to be completed.

The results shown in Figures 2 and 3 are obtained on the basis of a time increment equal to $\Delta t = 0.1$ time unit. This relatively large time increment turned out to be amply adequate to reach an acceptable accuracy in the calculations. This conclusion is based on several time increments that were used to assess the influence of Δt on the evolution of the flow and front

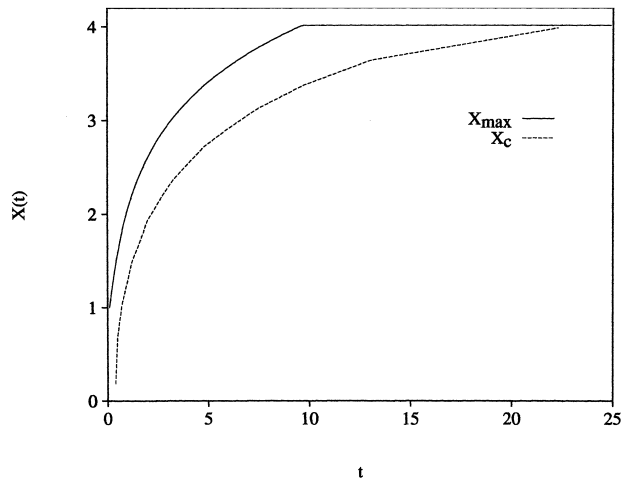

Figure 3. Evolution of the front tip position, X_{max}, and the contact point position, X_c, along the lateral walls with time for the transient flow problem in Figure 2.

with time. Calculations were carried out for the range for $0.05 \leq \Delta t \leq 0.1$. The evolution of the contact point position, $X_c(t)$, was monitored. It was clear from the results that the time increment has essentially no significant influence on the flow. However, this conclusion is valid for the time range of flow considered in this work. As expected, and as the figure indicates, the accuracy of the results begins to decrease when a relatively large time increment is used. The influence of mesh size was examined by varying the number of boundary elements, N. Three mesh sizes were considered, corresponding to $N = 80$, 160 and 320 elements. Again, no significant improvement was observed when a relatively high number of elements were used. This observation was valid over the whole range of time. Consequently, all results reported in this paper are based on $N = 80$.

The flow field at the front is further appreciated by examining the velocity components at the front, $U(y, t)$ and $V(y, t)$, along the x- and y-directions respectively. Figures 4 and 5 show the distributions of the axial and lateral components at different time stages between $t = 0.8$ and 25. The discrepancy between the velocity of the front tip and the points of contact is obvious from Figure 4, especially in the early stages. The figure shows, for instance, that $U(1, 0.8) \approx 0.9$, while $U(-0.5, 0.8) = U(2.5, 0.8) \approx 0.3$. This discrepancy decreases with time. The figure also shows that the velocity tends to generally converge in the long time everywhere including near the lateral walls. When the fluid touches the solid wall, there is an abrupt decrease (to zero) between the velocity of the moving part and the stagnant part as indicated by the 24.9 curve. The lateral velocity component, $V(y, t)$, is strongest initially, and is generally of the same order of magnitude as $U(y, t)$, as depicted from Figure 5. As expected, the lateral velocity vanishes at $y = -0.5$ and 2.5. However, there is a sharp drop in $V(y, t)$ near the lateral boundaries. It is also interesting to observe from Figure 5 that $V(y, t)$ is highly

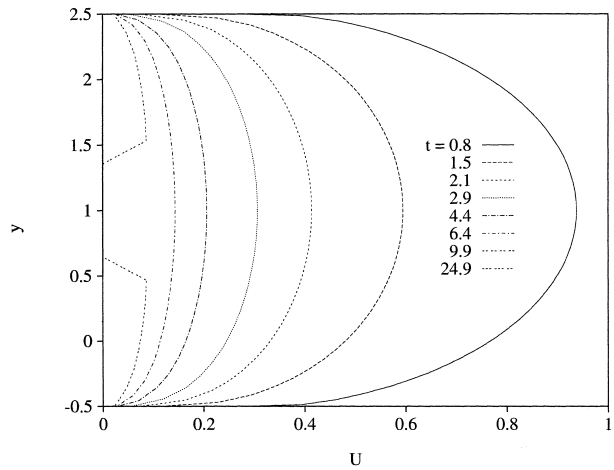

Figure 4. Distribution of the axial velocity component, $U(y, t)$, at the front for $0.8 < t < 25$, for the flow in Figure 3.

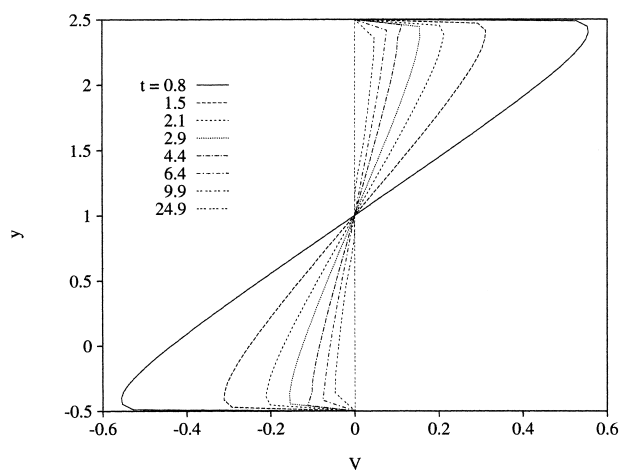

Figure 5. Distribution of the lateral velocity component, $V(y, t)$, at the front for $0.8 < t < 25$, for the flow in Figure 3.

non-linear near the walls, and is essentially linear in the bulk region. The overall non-linear behavior is further assessed in Figure 6, which shows the phase plots in the (U, V) plane for the same time stages as in Figures 4 and 5. The phase plots are closed orbits that are similar to those emerging from dynamical systems. They tend to decrease in the overall diameter, confirming the weakening of the flow with time.

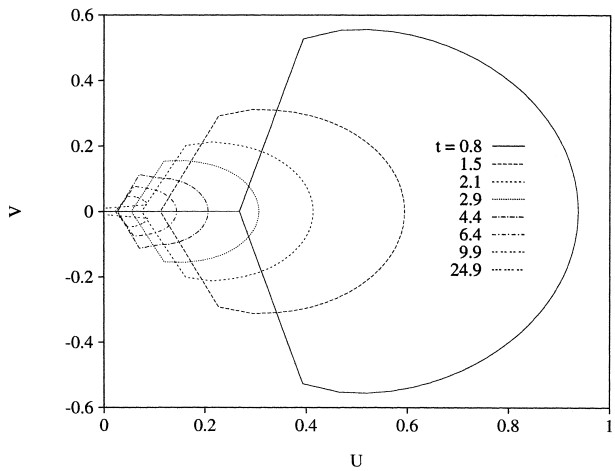

Figure 6. Phase plot of the axial and lateral velocity components, $U(y, t)$ and $V(y, t)$, at the front for $0.8 < t < 25$, for the flow in Figure 3.

4.2. Transient free-surface flow inside a curved cavity

The results on the flow inside a flat cavity in Figures 2 and 3 clearly illustrate the strong influence of the initial domain on the ensuing flow sequence. To this must be added the influence of the inlet flow pressure, which can be adjusted to compensate, for instance, the loss of flow near the lateral walls as indicated in Figure 3. However, this adjustment is not needed in this case given the slip at the lateral walls, which allows the flow at the walls to catch up with the flow in the middle region. In this section, the flow in a curved three-dimensional cavity is examined, which illustrates further the intricacies resulting from the influence of the inlet flow, the shape of the initial domain, and the slip at the lateral walls.

So consider the flow inside the curved parabolic cavity whose mid-surface is given by $z = -4/81x(x-6)(y-2.5)(y+0.5)$, where $(x, y) \in [0, 4] \times [-0.5, 2.5]$. Thus the maximum in z occurs at the point $(x = 3, y = 1)$ and is equal to 1. The region occupied initially by the fluid domain has a projection in the (x, y) plane given by $x = y(y-2)$ for $y \in [0, 2]$ as in the case of the flow inside the flat plate depicted in Figure 3. The resulting flow sequence is shown in Figure 7 for a period of 50 time units. The scale in the figure indicates the front at six successive unequal intervals. The remarkable feature of the flow is that, although the flow is very similar to that in the case of a flat plate (Figure 2), contact in this case occurs much later, which will become obvious once the projection on the (x, y) plane is examined. This suggests that the lateral flow is much weaker in this case. A more accurate assessment is obtained by examining the projections of the fronts onto the (x, y), (x, z) and (y, z) planes, which are shown in Figures 8–10 respectively. Figure 8 indicates clearly the difficulty of the fluid to come in contact with the lateral walls. In fact, all four corners take a relatively long time to be filled. This is reflected by the high density of curves along the edges in Figures 8–10. The evolutions of the front tip along x, $X_{\max}(t)$, that of the contact point, $X_c(t)$, and that of the maximum

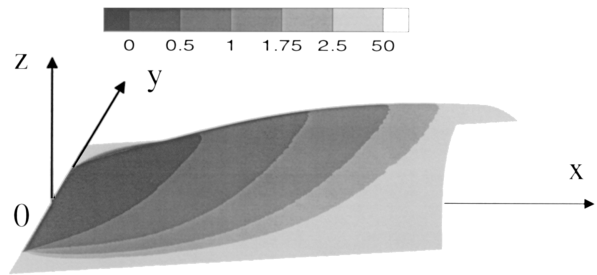

Figure 7. Transient flow inside a curved thin cavity. The fronts are shown at times $t = 0$, 0.5, 1.0, 1.75, 2.5 and 50 over a period of 50 time units.

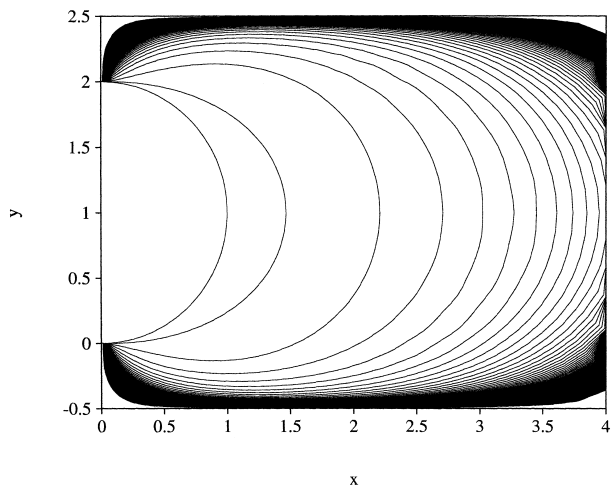

Figure 8. Projection of the fronts of transient flow in Figure 7 in the (x, y) plane.

height, $Z_{\max}(t)$, are shown in Figure 11. The results for $X_{\max}$ and X_c should be compared to those in Figure 3. It is interesting to observe that the behavior of $X_{\max}$ is essentially linear with time in the initial stages, similarly to the flow inside a flat plate (Figure 3). There is even a slight acceleration toward the end of the simulation. The contact point and the maximum height, on the other hand, tend to accelerate initially, eventually decelerating. Their rate of advance, however, remains higher than that of the front tip. The $Z_{\max}$ curve indicates that the maximum height is reached much earlier than the first contact with the lateral walls.

The flow field at the front is further appreciated by examining the velocity vector at the front. Figures 12 and 13 show the distributions of the axial and lateral components of the velocity at the fronts of Figure 7, $U(y, t)$ and $V(y, t)$ respectively. The profiles are shown over different time stages. The discrepancy between the velocity of the front tip, $U(1, t)$, and that

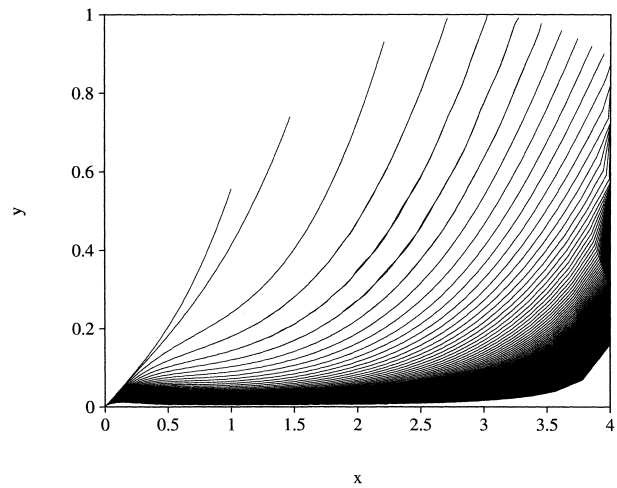

Figure 9. Projection of the fronts of transient flow in Figure 7 in the (x, z) plane.

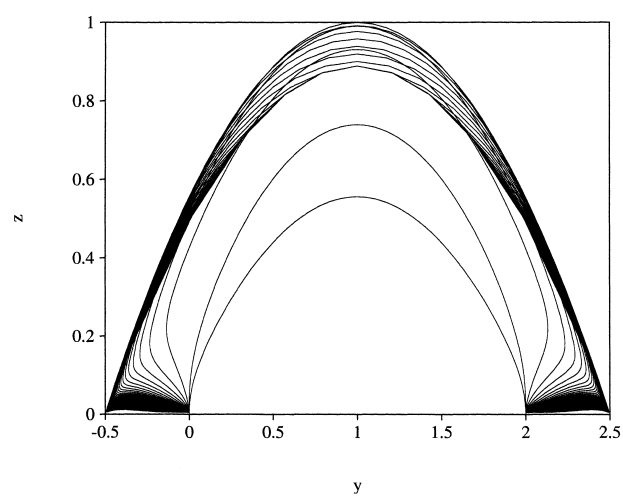

Figure 10. Projection of the fronts of transient flow in Figure 7 in the (y, z) plane.

of the points of contact is significant initially, but not as much in Figure 4. This discrepancy not only decreases with time, but the tip eventually begins to recede relative to the lateral walls. Although the velocity tends to generally converge in the long time everywhere, this rate of convergence is much smaller than in Figure 4. Similarly to Figure 5, the lateral velocity component, $V(y, t)$, is strongest initially, but is generally one order of magnitude smaller than

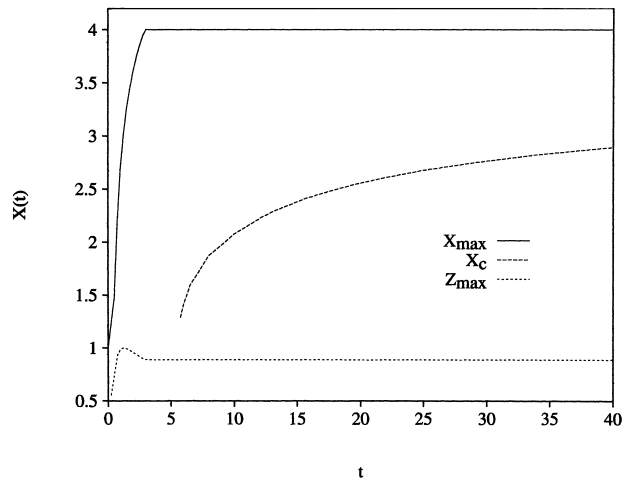

Figure 11. Evolution of the front tip position, X_{max}, the contact point position, X_c, along the lateral walls, and maximum height, Z_{max}, with time for the transient flow problem in Figure 6.

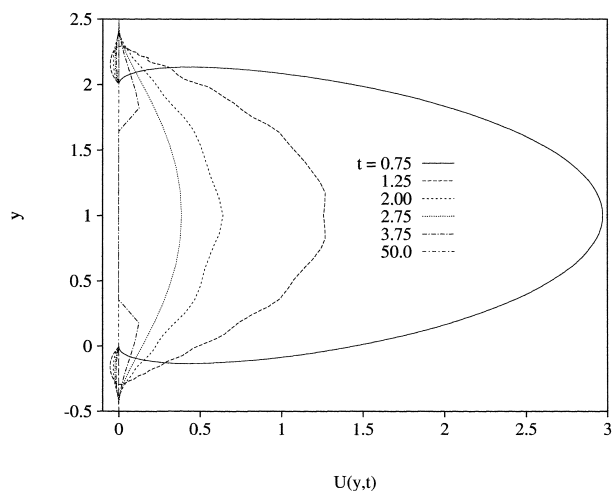

Figure 12. Distribution of the axial velocity component, $U(y, t)$, at the front for $0 < t < 50$, for the flow in Figure 7.

$U(y, t)$, as depicted from Figure 13. Although the lateral velocity vanishes at $y = -0.5$ and 2.5, there is no sharp drop in $V(y, t)$ near the lateral boundaries as in Figure 5. The overall non-linear behavior is further assessed in Figure 14, which shows the phase plot in the (U, V)

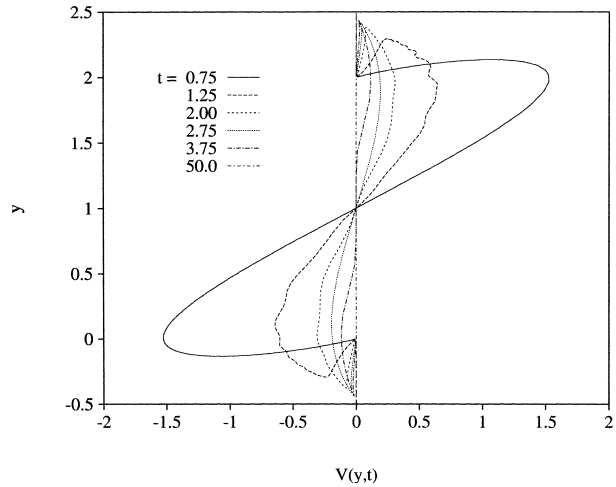

Figure 13. Distribution of the lateral velocity component, $V(y, t)$, at the front for $0 < t < 50$, for the flow in Figure 7.

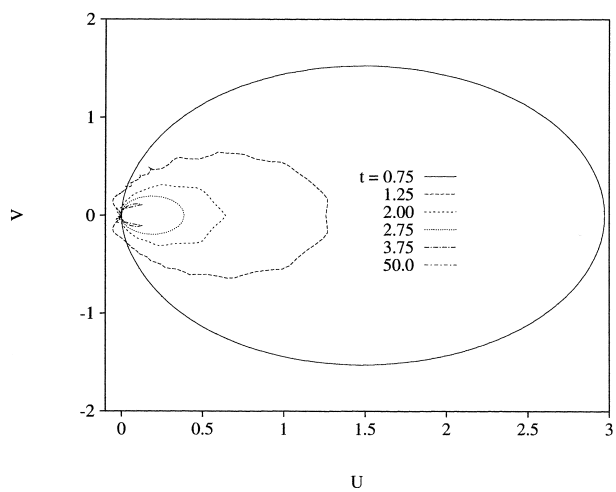

Figure 14. Phase plot of the axial and lateral velocity components, $U(y, t)$ and $V(y, t)$, at the front for $0 < t < 50$, for the flow in Figure 7.

plane. The phase plots are closed orbits. The orbits in the early stages are reminiscent of the limit cycle of a harmonic oscillator. They decrease in their overall diameter as in Figure 6, indicating a weakening in the flow. There is a growing distortion of the orbits, reflecting a growth in non-linearity with time, which is typically reflected by the $t = 3.75$ orbit.

5. CONCLUSION

The general lubrication formulation is extended for transient free-surface flows inside a three-dimensional thin cavity. A fully Lagrangian boundary element approach is used to solve the moving-boundary problem. In this work, inertia is neglected, and the pressure becomes independent of the height variable (z). Two transient free-surface flow configurations are examined. In both cases, the driving pressure gradient is parabolic and maintained fixed at the cavity entrance. First, the flow inside a flat plate with the fluid occupying initially a parabolic domain is studied. In this case, the flow in the middle region tends to accelerate initially relative to the flow at the lateral walls. However, the slip at the walls eventually renders the front straight again, leading to a plug-flow situation in the (x, y) plane. There is a strong lateral flow initially as indicated by the velocity distribution along the front. This flow, however, diminishes in intensity, leading to the straightening of the front with time. Secondly, the flow inside a curved cavity shows that the fluid tends to advance more rapidly than inside the flat plate. This results in a significant delay in the fluid contacting the lateral walls. The present work illustrates clearly the usefulness of the boundary element code to problems involving a complex three-dimensional geometry as encountered in the polymer processing industry.

ACKNOWLEDGMENTS

The support of the Natural Sciences and Engineering Council of Canada is gratefully acknowledged.

REFERENCES

1. Floryan JM, Rasmussen H. Numerical methods for viscous flows with moving boundaries. *Applied Mechanics Review* 1989; **42**: 323.
2. Nickell RE, Tanner RI, Caswell B. The solution of viscous incompressible jet and free-surface flows using finite element method. *Journal of Fluid Mechanics* 1974; **65**: 189.
3. Siliman WJ, Scriven LE. Separating flow near a static contact line: slip at a wall and shape of a free surface. *Journal of Computational Physics* 1980; **34**: 287.
4. Ruschak KJ. A method of incorporating free boundaries with surface tension in finite element fluid flow simulation. *International Journal for Numerical Methods in Engineering* 1980; **15**: 639.
5. Kawahara M, Miwa T. Finite element analysis of wave motion. *International Journal for Numerical Methods in Engineering* 1984; **20**: 1193.
6. Bach P, Hassager O. An algorithm for the use of the Lagrangian specification in Newtonian fluid mechanics and applications to free surface flows. *Journal of Fluid Mechanics* 1985; **152**: 173.
7. Ramaswany B, Kawahara M. Lagrangian finite element analysis applied to viscous free surface fluid flow. *International Journal for Numerical Methods in Fluids* 1987; **7**: 953.
8. Chipada S, Jue TC, Joo SW, Wheeler MF, Ramaswamy R. Numerical simulation of free-boundary problems. *Computational Fluid Dynamics* 1996; **7**: 91.
9. Peterson RC, Jimack PK, Kelmanson MA. The solution of two-dimensional free surface problems using automatic mesh generation. *International Journal for Numerical Methods in Fluids* 1999; **31**: 937.
10. Kim SO, No HC. Second order model for free surface convection and interface reconstruction. *International Journal for Numerical Methods in Fluids* 1998; **26**: 79.
11. Engelman MS, Sani R, Gresho PM. The implementaton of normal and/or tangential boundary conditions in finite element codes for incompressible fluid flow. *International Journal for Numerical Methods in Fluids* 1982; **2**: 225.
12. Mashayek F, Ashgriz N. A spline-flux method for simulating free surface flows. *Journal of Computational Physics* 1995; **122**: 367.

13. Martinz-Herrara JI, Derby JJ. Analysis of capillary-driven viscous flows during sintering of ceramic powders. *AIChE Journal* 1994; **40**: 1794.
14. Wilkes ED, Philips SD, Bassaran OA. Computational and experimental analysis of dynamics of droplet formation. *Physics of Fluids* 1999; **11**: 3577.
15. Levesque RJ, Li Z. Immersed interface methods for Stokes flow with elastic boundaries or surface tension. *SIAM Journal of Scientific Computing* 1997; **18**: 709.
16. Khayat RE, Luciani A, Utracki LA. Boundary-element analysis of planar drop deformation in confined flow. Part I. Newtonian fluids. *Engineering Analysis and Boundary Elements* 1997; **19**: 279.
17. Khayat RE, Huneault M, Utracki LA, Duquette R. A boundary element analysis of planar drop deformation in the screw channel of a mixing extruder. *Engineering Analysis and Boundary Elements* 1998; **21**: 155.
18. Khayat RE. Boundary-element analysis of planar drop deformation in confined flow. Part II. Viscoelastic fluids. *Engineering Analysis and Boundary Elements* 1998; **22**: 291.
19. Khayat RE, Luciani A, Utracki LA, Godbille F, Picot J. Influence of shearing and elongation on the deformation of drops in a convergent/divergent tube of Newtonian and viscoelastic fluids. *International Journal of Multiphase Flow* 1999; **26**: 17–44.
20. Khayat RE. Three-dimensional boundary-element analysis of drop deformation for Newtonian and viscoelastic systems. *International Journal for Numerical Methods in Fluids* 2000; **34**: 241–275.
21. Khayat RE. Deformation of a shear-thinning drop in Newtonian flow. *International Journal for Numerical Methods in Fluids* 2000; **33**: 559.
22. Khayat RE, Derdouri A, Hebert LP. A boundary-element approach to three-dimensional gas-assisted injection molding. *Journal of Non-Newtonian Fluid Mechanics* 1995; **57**: 253.
23. Khayat RE, Elsin W, Kim K. An adaptive boundary-element approach to transient free-surface flow as applied to injection molding. *International Journal for Numerical Methods in Fluids* 2000; **33**: 847.
24. Khayat RE, Raducanu P. A coupled finite element/boundary element approach for the three-dimensional simulation of air venting in blow molding and thermoforming. *International Journal for Numerical Methods in Engineering* 1998; **43**: 151.
25. Khayat RE, Derdouri A, Frayce D. Boundary-element analysis of three-dimensional transient mixing processes of Newtonian and viscoelastic fluids. *International Journal for Numerical Methods in Fluids* 1998; **28**: 815.
26. Khayat RE. A boundary-element analysis of 3D multiply-connected cavity mixing of polymer solutions. *International Journal for Numerical Methods in Fluids* 1999; **31**: 1173.
27. Khayat RE, Marek K. An adaptive boundary-element Lagrangian approach to 3D transient free-surface flow of viscous fluids. *Engineering Analysis and Boundary Elements* 1999; **23**: 111.
28. Wrobel LC. The dual reciprocity boundary element formulation for nonlinear problems. *Computational Methods in Applied Mechanical Engineering* 1987; **65**: 147.
29. Nowak AJ. Application of the multiple reciprocity method for solving nonlinear problems. In *Advanced Computational Methods in Heat Transfer II*, *Vol I: Conduction*, *Radiation and Phase Change*, Wrobel LC, Brebbia CA, Nowak AJ (eds). Computational Mechanics Publications: Southampton, 1995.
30. Neves AC, Brebbia CA. The multiple reciprocity boundary element method for transforming domain integrals to the boundary. *International Journal for Numerical Methods in Engineering* 1991; **31**: 709.
31. Frayce D, Khayat RE. A dual reciprocity boundary element approach to three-dimensional transient heat conduction as applied to materials processing. *Numerical Heat Transfer A* 1996; **29**: 243.
32. Tucker CL. *Computer Modeling for Polymer Processing*. Hanser Verlag: Munich, 1988.
33. Keunigs R. An algorithm for the simulation of transient flows with free surface. *Journal of Computational Physics* 1986; **62**: 199.
34. Khayat RE, Garcia-Rejon A. Uniaxial and biaxial unsteady inflation of a viscoelastic material. *Journal of Non-Newtonian Fluid Mechanics* 1992; **43**: 31.
35. Mao W, Khayat RE. Numerical simulation of transient planar flow of a viscoelastic materials with two moving free surfaces. *International Journal for Numerical Methods in Fluids* 1995; **21**: 1137.
36. Power H, Wrobel LC. *Boundary Integral Methods in Fluid Mechanics*. Computational Mechanics Publications: Southampton, 1995.

